NUMERICAL INVESTIGATION OF CHARACTIRISTICS OF DUAL-CIRCUIT NOZZLES WITH CONSIDERING THE EXTERNAL FLOW

M. B. Guzairov, I. A. Krivosheev, D. A. Akhmedzyanov, A. E. Kishalov, K. V. Markina
USATU – Ufa State Aviation Technical University, Russia

Introduction

Aircraft gas turbine engine – is the most difficult and laborious element of the aircraft. Its development and creation requires enormous time and labour resources. Exhaust arrangement of the jet engine are jet nozzles, the main purpose of which is the conversion of thermal and potential energy of the gas to kinetic energy of the jet stream.

One of the promising methods for studying the parameters and characteristics of the exhaust arrangement of aircraft engines (AE) is a three-dimensional numerical simulation of thermogas dynamic in a variety of software systems. To simulate the processes occurring in the air-gas channel of the AE one should use the ANSYS CFX - the best popular software.

The object of study in this article is the nozzle modeling of bypass turbojet engine with high bypass ratio on various operation modes with external flow considering. For the study the following input parameters were selected: 2 variants of geometry (Table 1) and 100 variants of the flow parameters (list of all possible combinations of the differential pressure at the nozzle are $\pi^*_{C\_I}$= (1,4; 1,8; 2,2; 2,6; 3,0), $\pi^*_{C\_II}$ = (1,4; 1,8; 2,2; 2,6; 3,0) and Mach number M = (0; 0,6; 0,8; 0,9), at constant temperature in the inner and outer contours T^*_I = 800 K, T^*_{II} = 300 K, Table 2) [1].

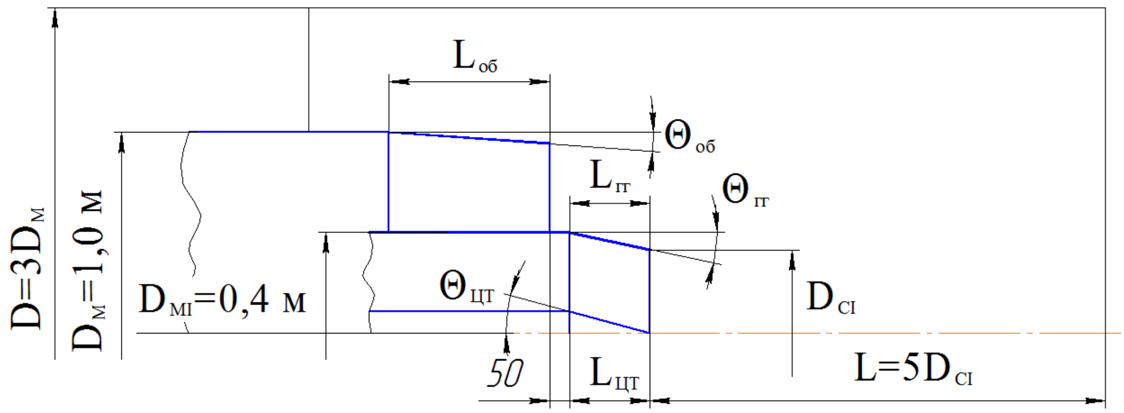

Fig. 1. Scheme of rated operating conditions

Table 1. Variants of geometry

Variant of geometry	Shell is the outer contour		Shell is the inner contour		Central body	
	Extension, deg.	Taper angle, grad	Extension, deg.	Taper angle, grad	Extension, deg.	Taper angle, grad
1	0,4	4	0,2	12	0,2	15
2	0,6	8	0,2	12	0,2	15

Table2. Variants of the flow parameters

Variant of the flow parameters	Inner contour	Outer contour	Mach	Variant of the flow parameters	Inner contour	Outer contour	Mach
	$\pi_c{}^*{}_I$	$\pi_c{}^*{}_{II}$	M_∞		$\pi_c{}^*{}_I$	$\pi_c{}^*{}_{II}$	M_∞
1	**2**	**3**	**4**	**5**	**6**	**7**	**8**
1	1,4	1,4	0	51	1,4	1,4	0,8
2	1,8			52	1,8		

1	2	3	4	5	6	7	8
3	2,2			53	2,2		
4	2,6			54	2,6		
5	3,0			55	3,0		
6	1,4			56	1,4		
7	1,8			57	1,8		
8	2,2	1,8		58	2,2	1,8	
9	2,6			59	2,6		
10	3,0			60	3,0		
11	1,4			61	1,4		
12	1,8			62	1,8		
13	2,2	2,2		63	2,2	2,2	
14	2,6			64	2,6		
15	3,0			65	3,0		
16	1,4			66	1,4		
17	1,8			67	1,8		
18	2,2	2,6		68	2,2	2,6	
19	2,6			69	2,6		
20	3,0			70	3,0		
21	1,4			71	1,4		
22	1,8			72	1,8		
23	2,2	3,0		73	2,2	3,0	
24	2,6			74	2,6		
25	3,0			75	3,0		
26	1,4			76	1,4		
27	1,8			77	1,8		
28	2,2	1,4		78	2,2	1,4	
29	2,6			79	2,6		
30	3,0			80	3,0		
31	1,4			81	1,4		
32	1,8			82	1,8		
33	2,2	1,8		83	2,2	1,8	
34	2,6			84	2,6		
35	3,0			85	3,0		
36	1,4			86	1,4		
37	1,8			87	1,8		
38	2,2	2,2	0,6	88	2,2	2,2	0,9
39	2,6			89	2,6		
40	3,0			90	3,0		
41	1,4			91	1,4		
42	1,8			92	1,8		
43	2,2	2,6		93	2,2	2,6	
44	2,6			94	2,6		
45	3,0			95	3,0		
46	1,4			96	1,4		
47	1,8			97	1,8		
48	2,2	3,0		98	2,2	3,0	
49	2,6			99	2,6		
50	3,0			100	3,0		

Technique of modeling in ANSYS CFX

In CAD system NX 8.0 the three-dimensional solid model was built (Fig. 1). The computational model is a sector of 20° (axisymmetric flow). Then, the model was imported into ANSYS. Next finite volume mesh was built on the three-dimensional model. Fig. 2 shows the mesh generated for the present configuration. In the model with the first variant of geometry the number of cells for this model is about 606 000 (Fig. 2a). In the model with the second variant of geometry the number of cells for this model is about 670 000 (Fig. 2b).

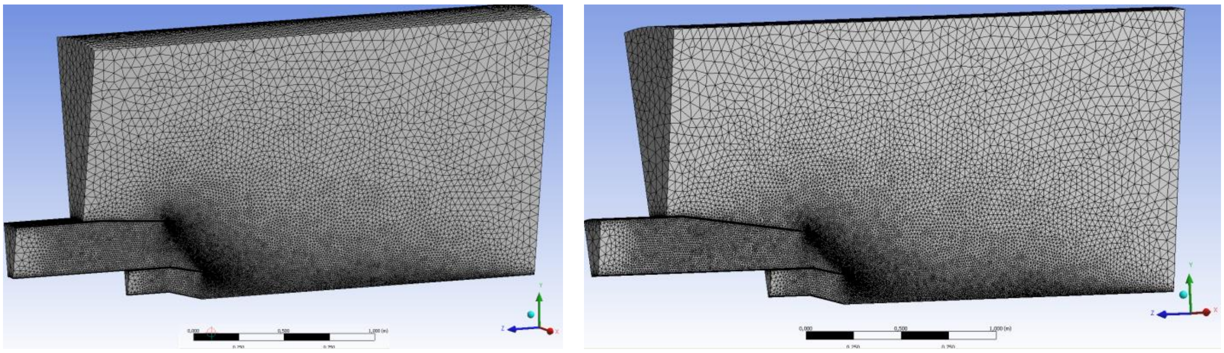

a b

Fig.2. Three dimensional view of the grid
(a – the first variant of geometry, b – the second variant of geometry)

After mesh generations it is necessary to install and configure the boundary conditions and laws calculation of CFX-Pre.

For simulation the Air Ideal Gas model, heat transfer model – Total Energy, turbulence model $k-\varepsilon$ are used. The reference pressure in the model is P_{ref}=101325 Pa.

Inlet boundary condition is the set at the entrance to the inner contour of the parameters: flow regime – Mixed, normal speed $V_{\text{вх\_I}}$, total overpressure $P^{*}_{\text{изб\_I}}$, total temperature T_{I}^{*}=800 K. Turbulence intensity (for all variants) was assumed equal to 5%.

Inlet boundary condition is the set at the entrance to the outer contour of the parameters: flow regime – Mixed, normal speed $V_{\text{вх\_II}}$, total overpressure $P^{*}_{\text{изб\_I}}$, total temperature T_{II}^{*}=300 K.

Opening - the boundary condition was set at the inlet to the outlet region to the outer flow with modeling parameters: overpressure $P_{\text{изб\_H}}$= 0 Pa, temperature T_{H} = 288 K (for M=0).

For the other variants (for $M\neq 0$) Inlet - the boundary condition was set at the inlet to the outlet domain with the parameters: speed V_{H} (corresponding Mach number), temperature 288 K. Opening the boundary condition was set on the outer border region and on the output from the model with the parameters: overpressure $P_{\text{изб\_H}}$= 0 Pa, temperature T_{H} = 288 K.

The axis of the 20°-sector model was assigned symmetry condition (Fig. 3).

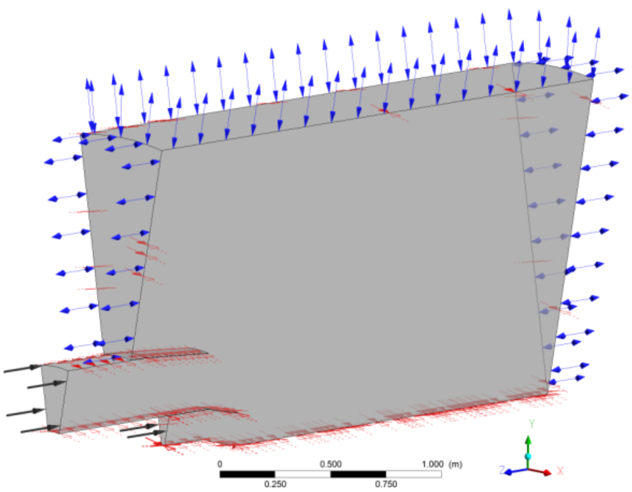

Fig. 3. Model with boundary conditions in CFX-Pre

Results of the simulation

Some results of modeling are shown below in Figures. In Fig. 4-6 results of modeling under the subcritical regime of the going out flows from the nozzles are shown, where there is a subsonic jet flows picture.

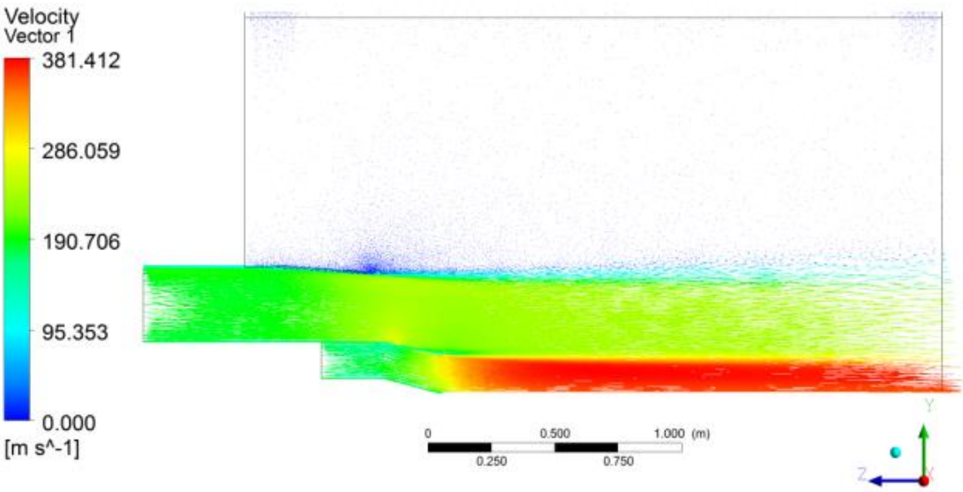

Fig. 4. Velocity field (the first variant of geometry, variant of the flow parameter – 1)

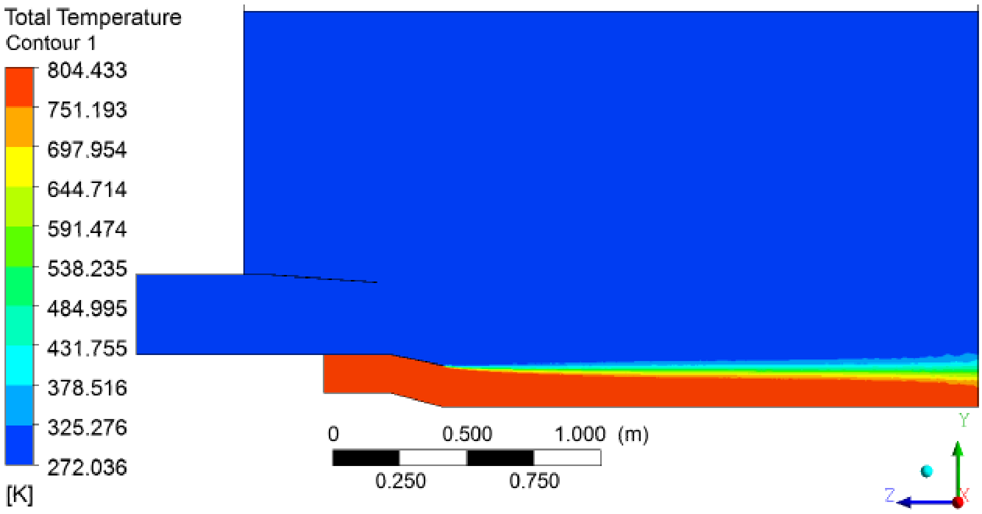

Fig. 5. Total temperature (the first variant of geometry, variant of the flow parameter – 1)

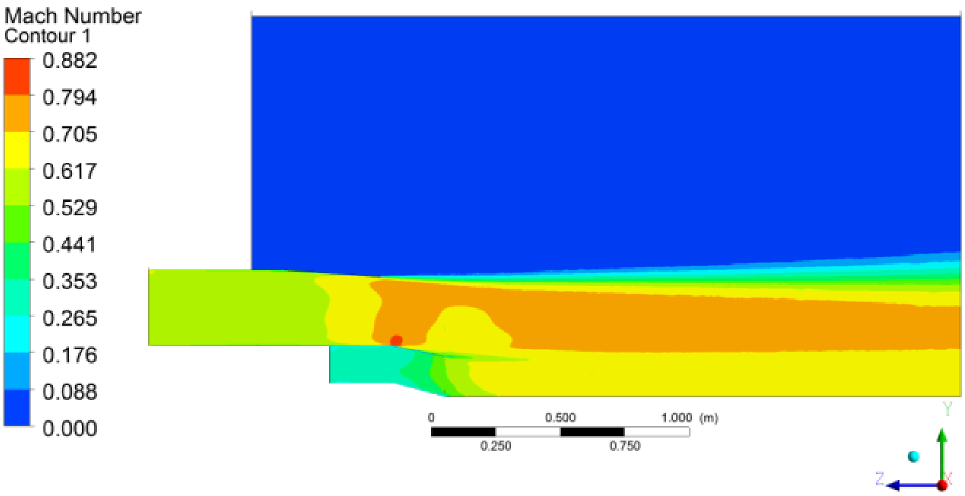

Fig. 6. Mach number (the first variant of geometry, variant of the flow parameter – 1)

Fig. 7-9 shows results of modeling under supercritical going out regimes where typical periodic structures - "rolls" are formed.

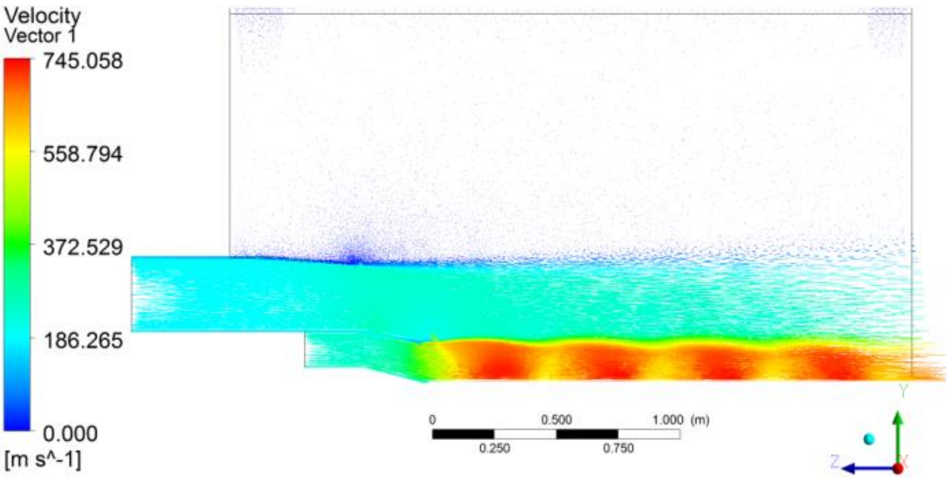

Fig. 7. Velocity field (the first variant of geometry, variant of the flow parameter – 5)

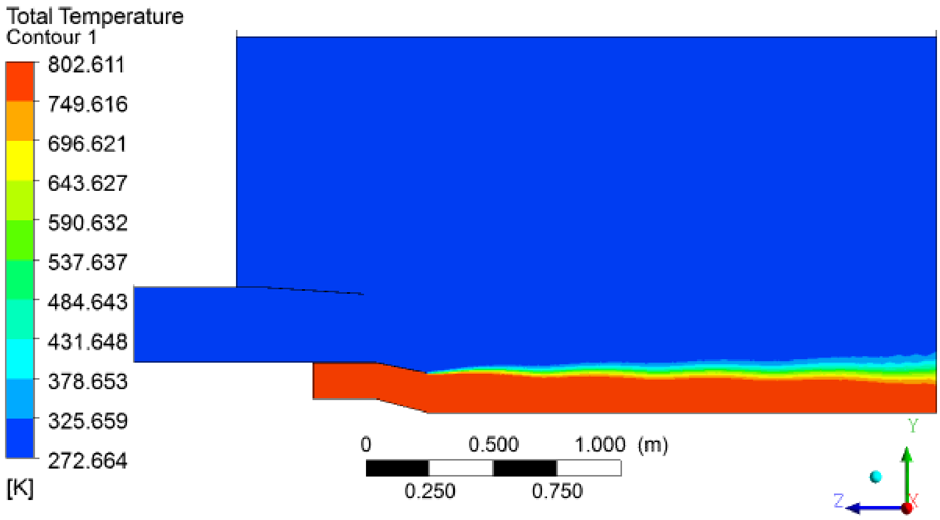

Fig. 8. Total temperature (the first variant of geometry, variant of the flow parameter – 5)

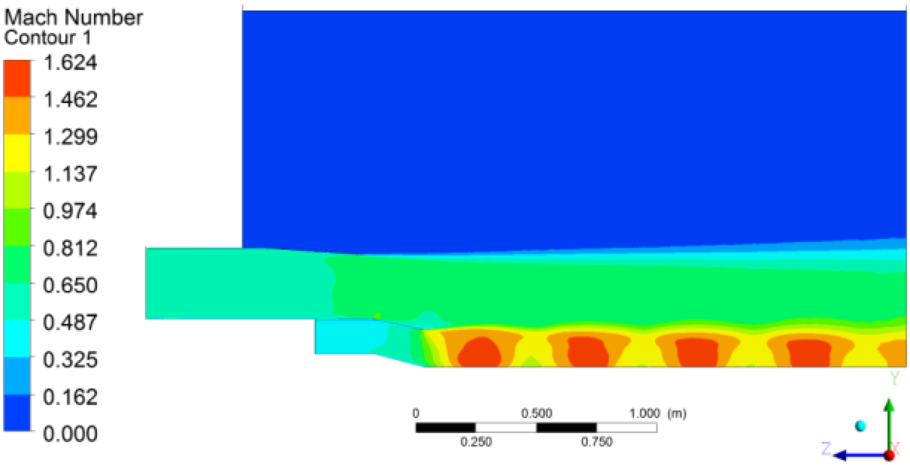

Fig. 9. Mach number(the first variant of geometry, variant of the flow parameter – 5)

Fig. 10-12 shows the flow structure deformation of the jet streams in the interaction of the inner and outer nozzles when supercritical modes.

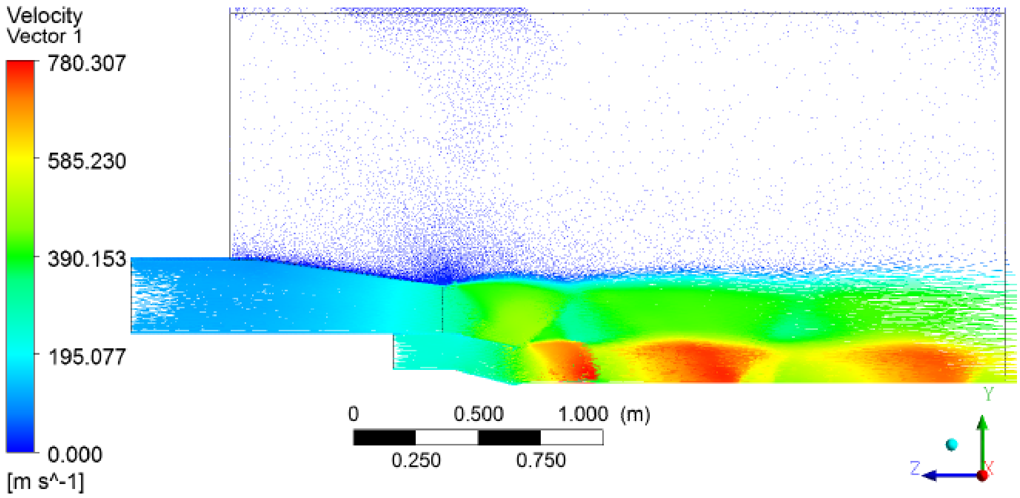

Fig. 10. Velocity field (the second variant of geometry, variant of the flow parameter – 25)

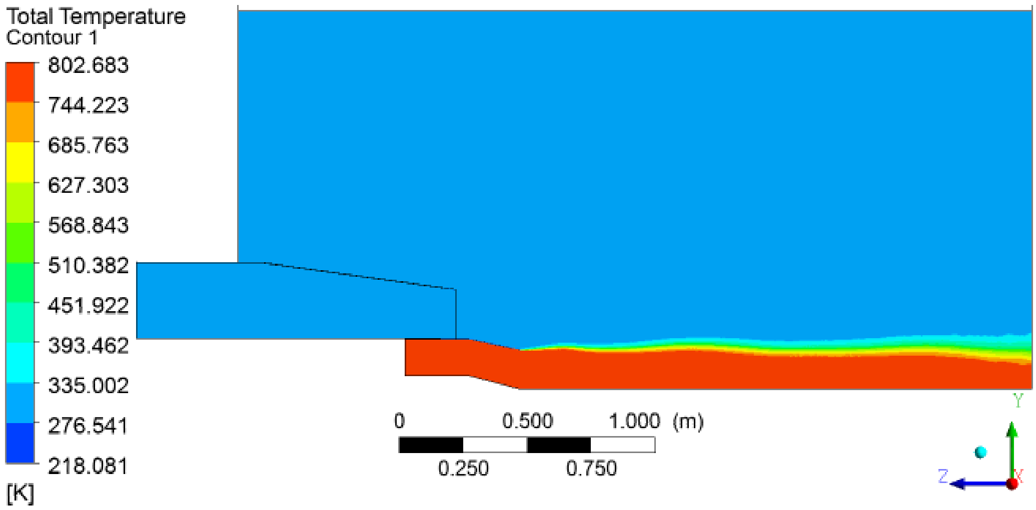

Fig. 11. Total temperature (the second variant of geometry, variant of the flow parameter – 25)

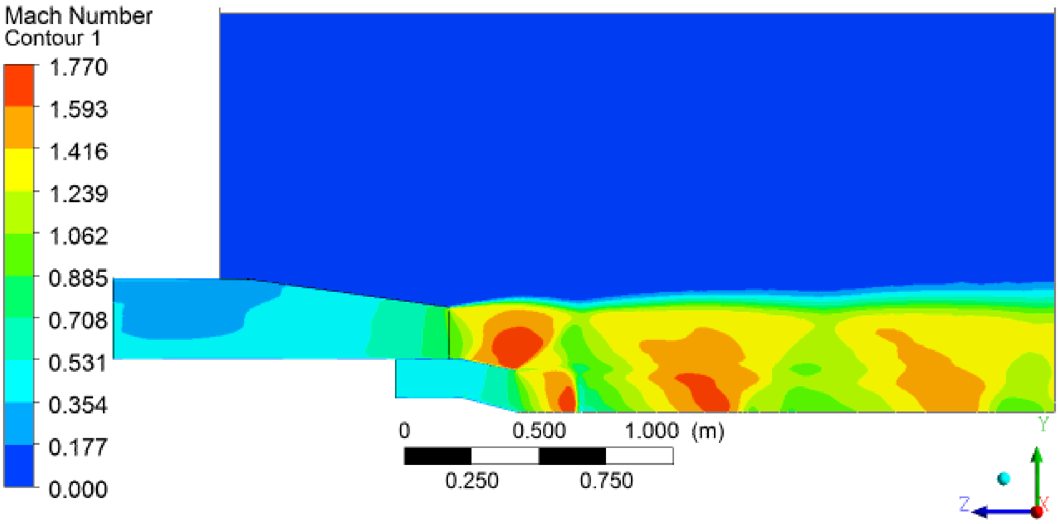

Fig. 12. Mach number (the second variant of geometry, variant of the flow parameter – 25)

By increasing of the outer flow velocity the flow structure also changes a little, it becomes more difficult (Fig. 13–15).

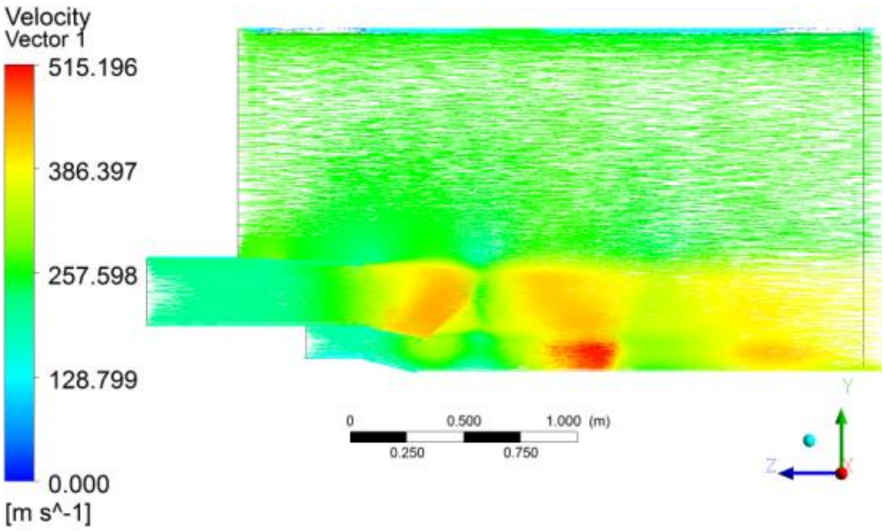

Fig. 13.Velocity field (the first variant of geometry, variant of the flow parameter – 66)

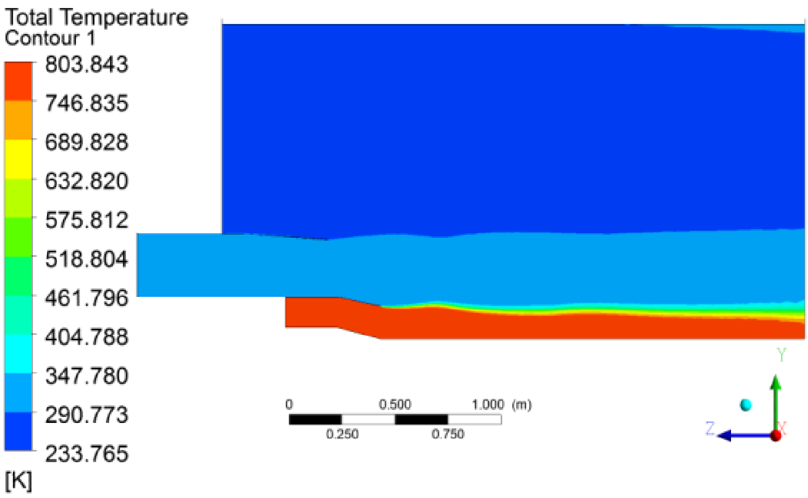

Fig. 14. Total temperature (the first variant of geometry, variant of the flow parameter – 66)

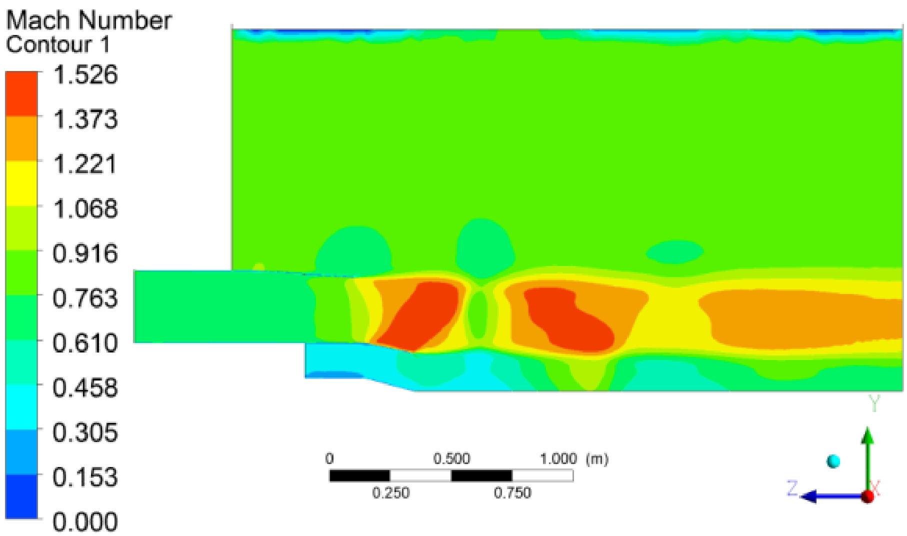

Fig. 15. Mach number(first variant of geometry, variant of the flow parameter – 66)

Method for determining the nozzles characteristics as the calculations results in ANSYS

Each calculation performed in ANSYS 13.0 CFX is processed with input and output measurements of such parameters as air flow rate in the inner and outer contours ($G_{\text{BX\_I}}$ and $G_{\text{BX\_II}}$), weight-average total pressure at the inlet to the inner and outer contours ($P^{*}_{\text{BX\_I}}$ and

$P^*_{вх\_II}$), weight-average pressure at the throat of the nozzle inner and outer contours ($P_{кр\_I}$ and $P_{кр\_II}$), weight-average velocity at the entrance to the inner and outer contour ($V_{вх\_I}$ and $V_{вх\_II}$), medium in size and pressure on the outer and inner surface of the nozzle inner loop ($P_{нар\_I}$ and $P_{внут\_I}$), medium area pressure on the outer and inner contour of the outer nozzle surface ($P_{нар\_II}$, $P_{внут\_II}$).

According to [2, 3], the flow coefficient is the ratio of real flow rate of the working substance to the ideal working fluid flow. The calculated values of the ideal and the real costs of air through the inner and outer nozzle flow coefficient is defined according to the following formulas:

$$\mu_{I} = \frac{G_{вх\_I}}{G_{вх\_It}}, \tag{1}$$

$$\mu_{II} = \frac{G_{вх\_II}}{G_{вх\_IIt}}. \tag{2}$$

According to the results calculations in ANSYS internal nozzles thrust is determined by formulas (3) and (4):

$$R_{I} = G_{вх\_I} V_{кр\_I} + F_{кр\_I} (P_{кр\_I} - P_{н}), \tag{3}$$

$$R_{II} = G_{вх\_II} V_{кр\_II} + F_{кр\_II} (P_{кр\_II} - P_{н}). \tag{4}$$

Total internal thrust of the outer and inner nozzle is determined by the formula (5):

$$R_{\Sigma} = R_{I} + R_{II}. \tag{5}$$

The resultant force is determined by the results of calculations in ANSYS, attached to the outer surface of the inner and outer nozzle formulas:

$$R_{нар\_I} = -\left(P_{внут\_I} - P_{нар\_I}\right) \cdot \pi \left({r^{нар}_{вх\_I}}^2 - {r^{нар}_{кр\_I}}^2 \right), \tag{6}$$

$$R_{нар\_II} = -\left(P_{внут\_II} - P_{нар\_II}\right) \cdot \pi \left({r^{нар}_{вх\_II}}^2 - {r^{нар}_{кр\_II}}^2 \right). \tag{7}$$

An effective internal and external nozzle thrust is determined by formulas (8) and (9):

$$R_{эф\_I} = R_{I} + R_{нар\_I}, \tag{8}$$

$$R_{эф\_II} = R_{II} + R_{нар\_II}. \tag{9}$$

Total effective thrust is determined by the formula (10):

$$R_{эф\_\Sigma} = R_{эф\_I} + R_{эф\_II}. \tag{10}$$

The inner thrust changing of the outer and inner nozzles is determined by the formulas:

$$\Delta R_{I} = R_{It} - R_{I}, \tag{11}$$

$$\Delta R_{II} = R_{IIt} - R_{II}. \tag{12}$$

Change in the effective external and internal thrust nozzles and their total effective thrust is determined by the formulas:

$$\Delta R_{эф\_I} = R_{эф\_It} - R_{эф\_I}, \tag{13}$$

$$\Delta R_{эф\_II} = R_{эф\_IIt} - R_{эф\_II}, \tag{14}$$

$$\Delta R_{эф\_\Sigma} = R_{эф\_\Sigma t} + R_{эф\_\Sigma}. \tag{15}$$

Method of calculating the ideal nozzle is shown in the article [4]. Table 3 and 4 shows the flow coefficient, internal thrust and efficiency thrust for variants I and II of geometry.

Table 3. Flow parameters in the first variant of geometry

Variant	μ_I	μ_{II}	R_I, N	R_{II}, N	ΔR_I, N	ΔR_{II}, N	$R_{эф\_I}$, N	$R_{эф\_II}$, N	$R_{эф\_\Sigma}$, N	$\Delta R_{эф\_I}$, N	$\Delta R_{эф\_II}$, N	$\Delta R_{эф\_\Sigma}$, N
1	**2**	**3**	**4**	**5**	**6**	**7**	**8**	**9**	**10**	**11**	**12**	**13**
1	0,928	0,946	4660,1	39713,3	93,3	152,2	3322,9	38516,6	41839,5	636,7	1029,3	1665,9
2	0,953	0,948	8895,8	40929,1	37,0	-154,7	6458,3	40101,1	46559,4	648,2	535,4	1183,6
3	0,949	0,948	13199,9	40912,9	-23,1	-157,9	9391,9	40083,2	49475,1	1237,2	530,0	1767,2
4	0,948	0,948	17317,0	40891,3	-35,7	-163,4	12078,3	40059,5	52137,8	1350,2	521,4	1871,6
5	0,943	0,948	21419,1	40862,5	-14,1	-169,8	14710,8	40028,0	54738,8	1516,7	510,7	2027,4
31	0,909	0,955	3775,1	72183,1	189,4	225,0	1991,4	69620,8	71612,2	776,8	1491,2	2268,0
32	0,927	0,955	8414,5	72331,7	240,7	217,5	5433,5	69712,4	75145,9	1187,2	1544,6	2731,8
33	0,950	0,955	12847,3	72287,2	23,6	204,3	8614,1	69693,3	78307,3	1285,4	1504,5	2789,9
34	0,948	0,955	17209,9	72281,1	-38,8	209,7	11577,6	69678,0	81255,6	1736,8	1519,1	3255,9
35	0,947	0,955	21442,3	72290,9	-74,9	187,4	14425,8	69697,6	84123,4	1784,4	1486,6	3271,0
56	0,909	0,955	3811,0	72389,9	162,2	-31,0	2030,2	69679,6	71709,8	751,6	1382,5	2134,0
57	0,927	0,955	8380,4	72302,9	237,6	13,4	5459,5	69432,3	74891,8	1101,8	1586,0	2687,8
58	0,950	0,955	12823,8	72633,8	27,4	-132,8	8726,2	69924,6	78650,8	1119,6	1282,9	2402,5
59	0,948	0,955	17195,1	72302,9	-39,1	-37,6	11660,6	69557,2	81217,8	1638,2	1409,1	3047,3
60	0,947	0,955	21467,2	72362,4	-72,6	-61,0	14562,0	69542,2	84104,3	1677,6	1461,0	3138,6
76	0,921	0,947	4200,6	38112,0	133,8	-169,5	3183,0	36267,3	39450,3	125,7	1068,9	1194,5
77	0,929	0,946	8732,0	38462,6	225,9	-547,6	6562,8	36682,2	43245,0	603,4	622,4	1225,8
78	0,949	0,947	13104,2	38048,4	-24,4	-131,3	9490,0	36421,8	45911,9	1036,6	885,0	1921,6
79	0,946	0,947	17376,1	38940,4	-41,2	-259,9	12269,4	37321,5	49590,8	1212,1	851,9	2063,9
80	0,946	0,947	21632,7	39523,5	-134,9	-581,8	15110,9	37837,6	52948,5	1232,9	632,7	1865,5

Table 4. Flow parameters in the second variant of geometry

Variant	μ_I	μ_{II}	R_I, N	R_{II}, N	ΔR_I, N	ΔR_{II}, N	$R_{эф\_I}$, N	$R_{эф\_II}$, N	$R_{эф\_\Sigma}$, N	$\Delta R_{эф\_I}$, N	$\Delta R_{эф\_II}$, N	$\Delta R_{эф\_\Sigma}$, N
1	**2**	**3**	**4**	**5**	**6**	**7**	**8**	**9**	**10**	**11**	**12**	**13**
1	0,942	0,933	4428,6	24073,6	76,1	740,6	3229,5	17134,8	20364,3	337,3	4030,1	4367,3
2	0,943	0,933	8980,0	24066,2	110,1	743,4	6560,7	17123,6	23684,3	803,0	4028,8	4831,7
3	0,942	0,933	13311,1	24065,8	60,6	740,2	9512,2	17121,7	26633,9	1295,5	4020,6	5316,1
4	0,942	0,933	17452,5	24065,5	38,2	735,7	12217,7	17118,7	29336,4	1396,9	4010,2	5407,2
5	0,942	0,933	21537,8	24064,1	-26,1	731,0	14846,6	17114,1	31960,7	1474,1	3998,4	5472,5
26	0,938	0,933	4321,3	23876,9	87,0	562,1	3231,1	16117,6	19348,7	188,9	4112,6	4301,5
27	0,949	0,933	8852,1	23637,2	64,4	648,5	6557,3	15944,7	22502,1	518,6	3958,2	4476,8
28	0,949	0,933	13122,7	23775,1	-26,8	550,4	9487,9	15265,1	24753,0	1056,0	4723,1	5779,1
29	0,949	0,933	17311,1	23785,9	-56,8	571,5	12226,2	16148,0	28374,2	1172,5	3904,7	5077,3
30	0,948	0,933	21301,2	23697,3	-106,9	605,6	14766,1	15995,2	30761,3	1257,5	3943,6	5201,0
51	0,936	0,933	4261,9	23325,7	90,4	574,4	3246,6	14907,9	18154,5	89,6	4165,3	4254,9
52	0,949	0,932	8796,8	23209,3	62,6	497,4	6631,7	14670,3	21302,0	337,2	3940,3	4277,5
53	0,949	0,932	13111,0	23189,6	-36,8	601,1	9556,6	14870,9	24427,5	964,1	3940,7	4904,8
54	0,948	0,932	17211,5	23305,9	-33,1	429,5	12287,9	14528,8	26816,7	1030,4	4152,9	5183,3
55	0,948	0,932	21658,5	23091,6	-170,4	602,9	15193,9	14850,8	30044,7	1137,6	3729,0	4866,6
81	0,874	0,934	3559,4	42403,4	194,9	1013,9	2601,7	24292,5	26894,2	-143,5	10575,5	10432,0
82	0,943	0,934	8323,1	41662,9	120,7	1053,2	6171,8	23877,7	30049,5	118,2	10252,1	10370,3
83	0,949	0,934	12898,5	41551,8	-0,7	1331,6	9315,3	24109,2	33424,5	671,3	10196,3	10867,7
84	0,948	0,934	17236,9	41947,2	-57,6	1276,7	12267,6	24297,9	36565,5	1054,5	10366,3	11420,8
85	0,949	0,934	21392,0	42099,3	-85,3	1091,9	15147,5	24366,2	39513,7	997,2	10263,5	11260,8
86	0,585	0,935	3241,9	59891,6	785,8	2799,6	1044,9	32988,3	34033,2	1813,1	12632,1	14445,2

Analysis of simulation results

The obtained simulation results qualitatively and quantitatively correspond to processes characteristic expiration flows from separate nozzles aircraft engines with high bypass. Changes in the flow coefficient depending on the pressure drop in the inner and outer nozzles and external flow velocity is shown in Fig. 16-19. For some calculations (II variant geometry, parameter variants 11, 36, 61, 81 и 86) the low values flow coefficients for the inner nozzle.

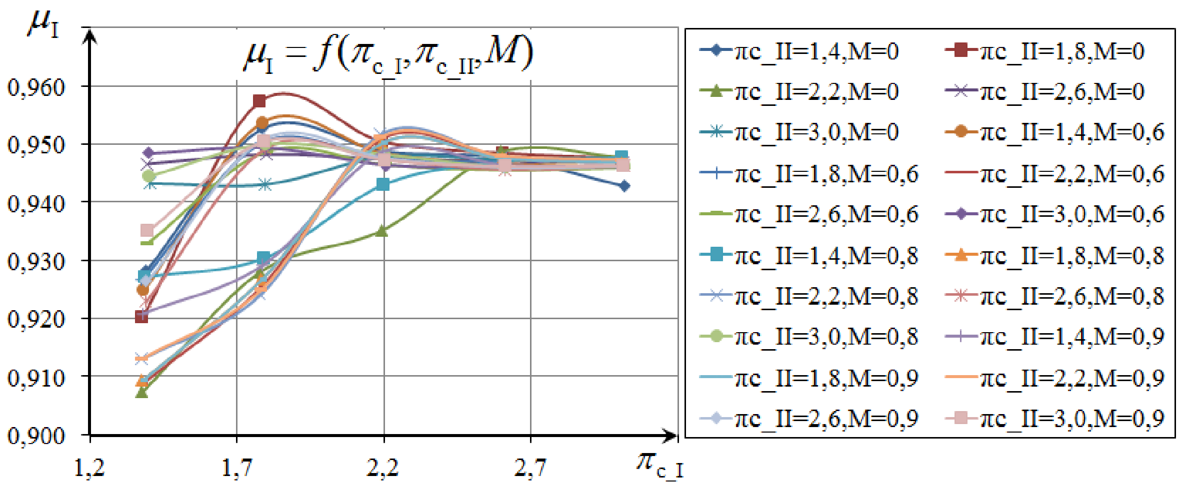

Fig. 16. The flow rate changing of the inner nozzle in dependence on the pressure drop and the external flow velocity, the first variant of geometry

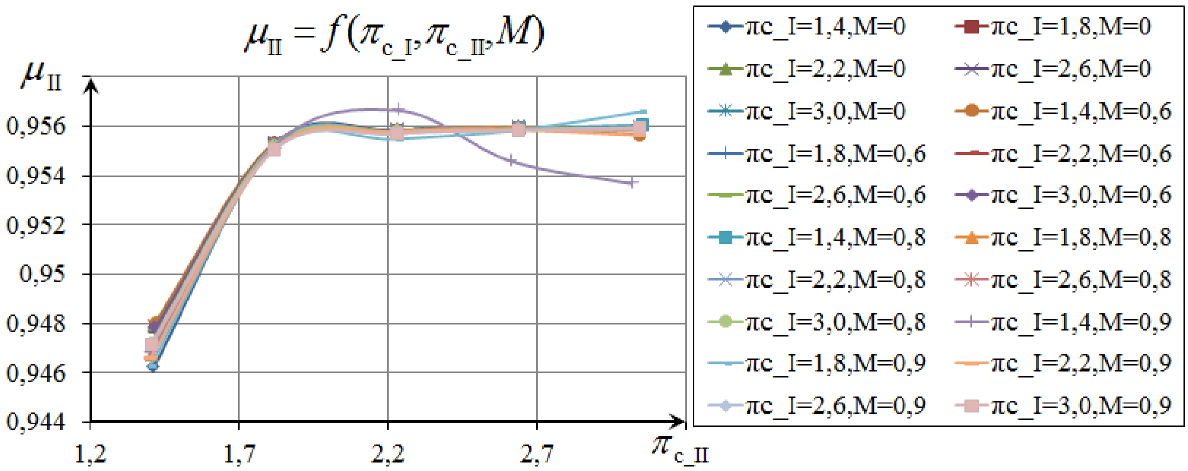

Fig. 17. The flow rate changing of the outer nozzle in dependence on the pressure drop and the external flow velocity, the first variant of geometry

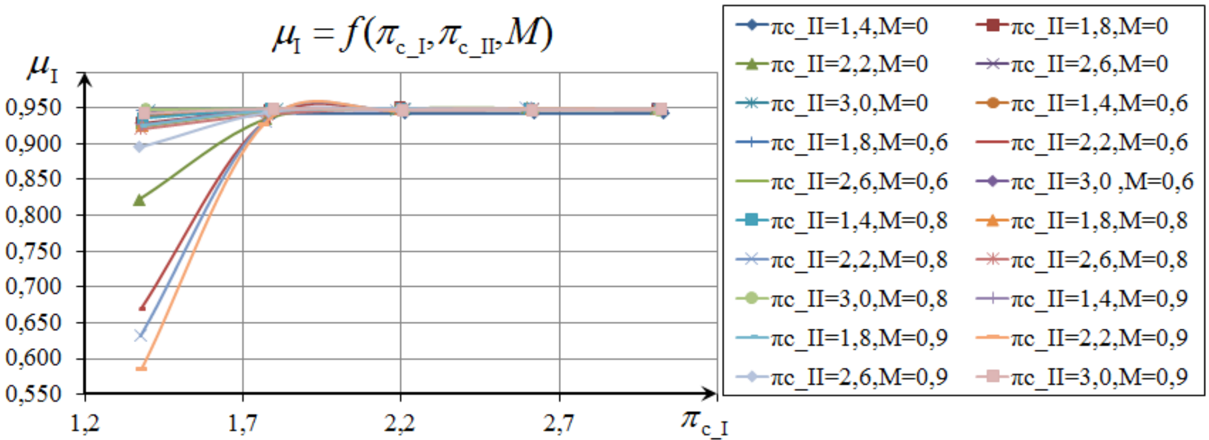

Fig. 18. The flow rate changing of the inner nozzle in dependence on the pressure drop and the external flow velocity, the second variant of geometry

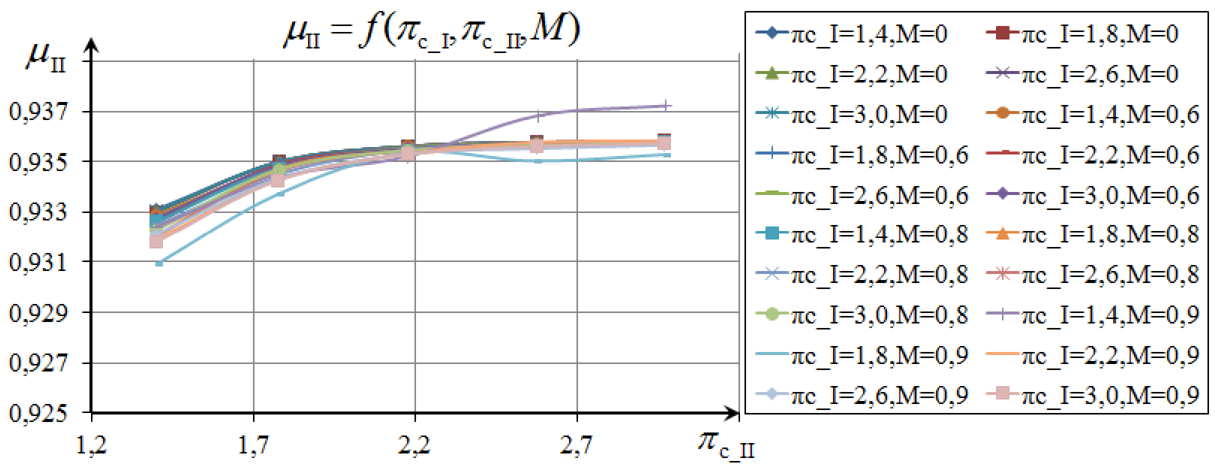

Fig. 19. The flow rate changing of the outer nozzle in dependence on the pressure drop and the external flow velocity, the second variant of geometry

In the calculations it is obtained that the change in the internal thrust ΔR_I (depending on the pressure drop across the nozzle) is insignificant. Negative values ΔR_I (thrust of the ideal nozzle is smaller than of the real) are explained by the ejection flow ΔR_I inner contour outer. The internal thrust changing of outer nozzle ΔR_{II} is much more substantial and ΔR_{II} increases with pressure drop across the nozzle outer contour.

Effective thrust $\Delta R_{эф\_I}$, $\Delta R_{эф\_II}$ change (loss) increases with pressure drop in the nozzles.

Conclusion

The developed method of processing the modeling results and method of determining the main nozzles characteristics allow preparing input data for calculations in ANSYS CFX, processing of the calculations results and determining of the main nozzle characteristics.

The calculation results and definite flow characteristics can be used for designing new and modernizing existing successfully exploited AE with separate nozzles and a large bypass ratio.

The developed methods and the results will allow creating of the groundwork for optimization of the flow characteristics of advanced AE and aircraft in various modes of operation allow you to achieve higher levels of excellence designed AE.

References

[1] Krivosheev I.A. Dual-circuit nozzle characteristics numerical investigation with separate outflow if external flow is avalible / Krivosheev I.A., Akhmedzanov D.A., Kishalov A.E., Markina K.V.// *Youth herald USATU*. No. 2 (7), pp 25-36, 2013.

[2] Shlyhtenko S.M. Theory and calculation air-breathing jet engine. *Textbook for university* – Moscow: MASHINOSTROENIE, 1987.

[3] LavruhinG.N. Aerodynamics jet nozzle. V.1. Internal characteristics nozzle. – Moscow, "Nauka", 2003

[4] KishalovA.E., Markina K.V. Calculation of characteristics of exhaust arrangement turbojet. *Youth herald USATU*. No. 4, pp 81-92, 2012.